NOTES AND CORRESPONDENCE

A Comparison of NEXRAD WSR-88D Radar Estimates of Rain Accumulation with Gauge Measurements for High- and Low-Reflectivity Horizontal Gradient Precipitation Events

GERARD E. KLAZURA

Environmental Research Division, Argonne National Laboratory, Argonne, Illinois

JESSICA M. THOMALE

Oklahoma Climatological Survey, University of Oklahoma, Norman, Oklahoma

D. SCOTT KELLY

National Weather Service, Melbourne, Florida

PAUL JENDROWSKI

National Weather Service, Honolulu, Hawaii

16 June 1998 and 26 March 1999

ABSTRACT

Radar-estimated rainfall amounts from the NEXRAD Weather Surveillance Radar precipitation accumulation algorithm were compared with measurements from numerous rain gauges (1639 radar versus gauge comparisons). Storm total rain accumulations from 43 rain events from 10 radar sites were analyzed. These rain events were stratified into two precipitation types: 1) high-reflectivity horizontal gradient storms and 2) low-reflectivity horizontal gradient events. Overall, the radar slightly overestimated rainfall accumulations for high-reflectivity gradient cases and significantly underestimated accumulations for low-reflectivity gradient cases. Varying degrees of range effects were observed for these two types of precipitation. For high-reflectivity gradient cases, the radar underestimated rainfall at the nearest ranges, overestimated at the middle ranges, and had fairly close agreements at the farthest ranges. A much stronger range bias was evident for low-reflectivity gradient cases. The radar underestimated rainfall by at least a factor of 2 in the nearest and farthest ranges, and to a somewhat lesser extent at midranges.

1. Introduction

Radar-estimated rainfall amounts from the NEXRAD Weather Surveillance Radar-1988 Doppler (WSR-88D) precipitation accumulation algorithm (Fulton et al. 1998; NOAA 1991) were compared with measurements from numerous rain gauges. Comparisons were performed by using ratios of gauge-measured to radar-estimated rainfall accumulations (G/R ratios).

Storm total rain accumulations from 43 rain events from 10 radar sites were analyzed. Storm total gauge amounts were compared with radar-estimated rainfall amounts at a single data file ''bin'' collocated above the gauge for similar time intervals. There were 1639 radar versus gauge comparisons. These rain events were stratified into two precipitation types: 25 high-reflectivity horizontal gradient storm events and 18 low-reflectivity horizontal gradient events. These procedures provided a dramatic improvement over previous WSR-88D radar–gauge comparisons (Manion and Klazura 1993) that used the standard graphics display of the Storm Total Precipitation product (Klazura and Imy 1993) with only 16 precipitation accumulation data levels and approximately 1-in. resolution.

This study was conducted in a semiquantitative manner to assess the performance of the WSR-88D precipitation accumulation algorithm in a general sense. It was not meant to be a rigorously objective scientific and statistical experiment. However, the strong differences that emerged between high-reflectivity gradient and low-reflectivity

Corresponding author address: Gerard Klazura, ABLE Project Office, 13645 SW Haverhill Rd., Augusta, KS 67010.
E-mail: jklazura@anl.gov

TABLE 1. Listing of the sites and number of high-reflectivity gradient (HRG) and low-reflectivity gradient (LRG) cases used in analyses. The letters in parentheses are the station identifiers used in Tables 2 and 3.

Sites		Number of cases	
		HRG	LRG
Cleveland, OH	(CLE)	9	3
Oklahoma City, OK	(OKC)	5	5
Boston, MA	(BOS)	4	4
Atlanta, GA	(ATL)	1	3
Chicago, IL	(CHI)		3
Denver, CO	(DEN)	2	
Houston, TX	(HGX)	1	
Norman, OK	(NOR)	1	
Lubbock, TX	(LBB)	1	
Phoenix, AZ	(PHX)	1	
Totals		25	18

gradient cases suggest that reasonably high confidence can be placed on the overall conclusions.

Standard operational quality control procedures were followed. Quality control of the radar reflectivity data is described in Fulton et al. (1998). An attempt was made to perform a basic level of quality control of gauge–radar pairs by excluding any nonraining pairs, that is, any pairs in which either the gauge or radar rainfall was below a minimum threshold (0.03 in. was used as threshold). For example, this would remove any pairs in which the gauge received rain but did not record it due to hardware problems or inaccurate timing and location specifications (e.g., a mismatch of radar and gauge clocks or errors in gauge latitude–longitude locations). Also, the pair would be excluded if the radar overshot the rain clouds at long ranges, while the gauge recorded rainfall properly.

2. Analyses procedures and data

Radar base reflectivity PPI plots (0.5° tilt) and storm total precipitation plots (Klazura and Imy 1993) from 10 U.S. WSR-88D sites (listed in Table 1) were analyzed for 59 rain events. The magnitudes, gradients, and patterns of radar reflectivity and radar-estimated rain accumulation were considered in assigning each case as a specific precipitation type. The description of the precipitation type represents a very general characterization of the dominant radar reflectivity and radar-estimated total precipitation structures as determined from a semiquantitative visual analysis.

Each precipitation event was assigned to one of four precipitation-type categories: 1) high-reflectivity gradient, 2) early high-reflectivity gradient–later low-reflectivity gradient, 3) low-reflectivity gradient with embedded high-reflectivity gradient, and 4) low-reflectivity gradient. Categories 2 and 3 include characteristics of both high-reflectivity gradient and low-reflectivity gradient, with varying spatial and temporal influences of each, and were therefore eliminated from further analyses.

The intent for this study was to isolate cases that were primarily either high-reflectivity gradient or low-reflectivity gradient in nature throughout the lifetime of the precipitation event (greater than 90% temporally). The high-reflectivity gradient category is characterized by substantial reflectivity cores exceeding 40–60 dB*Z*, with sharp reflectivity gradients adjacent to the cores. It has cores of radar-estimated storm total precipitation that are 5 to 10 times greater than the general accumulations over the area and that also have very sharp gradients. Figure 1 illustrates an example of a high-reflectivity gradient case as depicted on the storm total precipitation product (Fig. 1a) for the Oklahoma City WSR-88D for a 6-h, 21-min duration on 4 November 1994, and the base reflectivity product (Fig. 1b) for a radar scan within this time interval.

The low-reflectivity gradient category is characterized by fairly widespread reflectivities generally 25–40 dB*Z* with weak reflectivity gradients. The radar-estimated storm total precipitation products indicate weak gradients and areas of maximum precipitation, which are generally less than five times greater than the general accumulations over the area. Figure 2 illustrates an example of a low-reflectivity gradient case as depicted on the storm total precipitation product (Fig. 2a) for the Oklahoma City WSR-88D for a 9-h, 53-min duration on 29 April 1994, and the base reflectivity product (Fig. 2b) for a radar scan within this time interval. The higher rainfall accumulations depicted in the ring from about 30 to 60 n mi (Fig. 2a) may be due to enhanced reflectivities related to brightband effects.

Sixteen cases fell into categories 2 and 3 and were thus eliminated, leaving 25 high-reflectivity gradient cases and 18 low-reflectivity gradient cases for further analyses. Table 1 shows how these were distributed among the ten WSR-88D sites.

Rain gauge data from numerous gauges were provided by combinations of National Weather Service Forecast Offices, ALERT networks, and private rain gauge networks.

Digital WSR-88D data files of precipitation accumulation were produced either by processing archived radar reflectivity tapes with the precipitation accumulation algorithm after the precipitation event or by saving the precipitation accumulation data files immediately after the precipitation event at the site. Standard operational adaptable parameters (Fulton et al. 1998) were used in all cases, including the use of the *Z–R* relationship

$$Z = 300R^{1.4},$$

where Z has units of $\text{mm}^6\ \text{m}^{-3}$ and R is in $\text{mm}\ \text{h}^{-1}$. By using these data files, the analytical procedure generated a 5×5 matrix of ''bins'' of radar-derived storm total rainfall accumulation depth centered over each gauge. Each of the 25 bins has a spatial resolution of 2-km

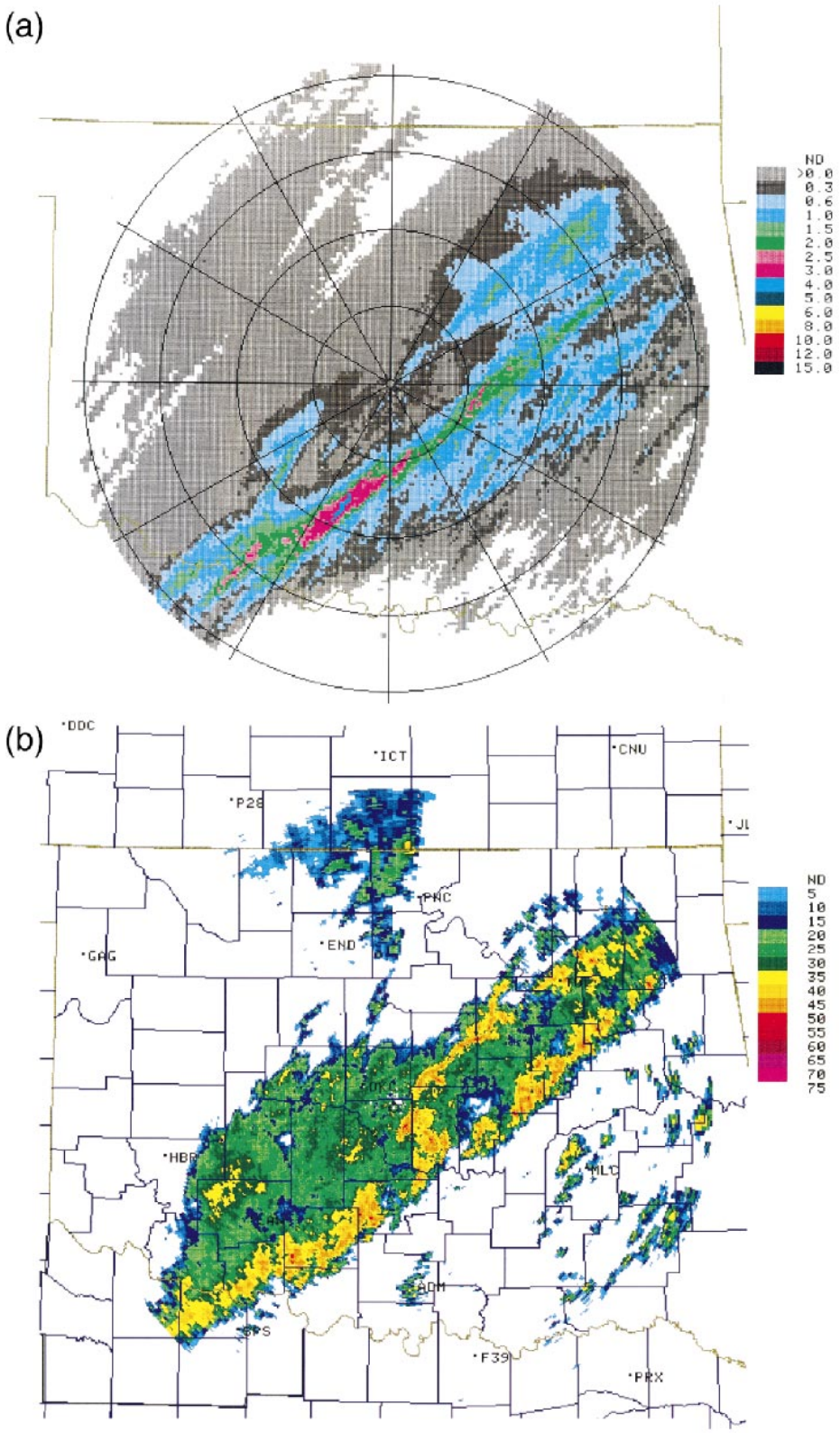

FIG. 1. (a) Oklahoma City, OK, WSR-88D storm total precipitation and (b) base reflectivity products on 4 Nov 1994 for range coverage of 124 n mi (230 km). (a) 1136–1757 UTC. Resolution is 1.1 n mi × 1.1 n mi (2 km × 2 km). Maps displayed are range rings at 30 n mi (55.65 km) intervals, radial sector

radial distance by 1° azimuth angle (about 2 km × 2 km at 115-km range from radar) and an accumulation resolution of 0.01 in. The width of the 1° bin varies from about 0.3 km at close ranges (20 km) to 4 km at the maximum range (230 km) of radar rainfall estimates (Fulton et al. 1998).

For this study, the radar bin that was selected to be compared with each gauge is the bin collocated with the gauge (closest to the latitude and longitude of the associated gauge) and located in the center of the 5 × 5 matrix of bins.

A valid gauge–radar pair is defined as a pair in which *both* the gauge and radar accumulation values are 0.03 in. or more. Smaller accumulations were omitted in order to remain generally consistent with the concept used by the radar bias calculations in the precipitation adjustment algorithm (Fulton et al. 1998; NOAA 1991) and to reduce errors caused by the minimum precipitation threshold of the rain gauge.

Valid gauge–radar pairs were converted into G/R ratios by using the method defined in Eq. (1):

$$G/R = \frac{\sum_{i=1}^{N} G_i}{\sum_{i=1}^{N} R_i}, \tag{1}$$

where N is the number of gauge–radar pairs, G_i is the ith gauge measured storm total rain amount, and R_i is the radar-estimated storm total rain amount for the 1° × 2 km bin collocated with the ith gauge. The G/R ratio is a mean radar bias factor defined as the sum of the observed amounts at all gauges with rainfall divided by the sum of the radar estimates for those gauges (Wilson and Brandes 1979). A bias factor greater (less) than 1.0 indicates that the radar has underestimated (overestimated) the rainfall. The G/R ratios were not computed unless there were at least nine valid gauge–radar pairs (i.e., both had values of at least 0.03 in.). Nine pairs were subjectively selected with the intent of making sure a reasonable sample size existed.

3. Results

Table 2 summarizes the G/R ratios and rainfall accumulation characteristics for each of 43 precipitation events. Other supporting information is also included (e.g., precipitation type, characteristic gauge amounts, storm duration, and date). The column labeled ''number of gauges'' indicates the number of gauges with valid precipitation that was considered versus the total number of gauges in the network. The entries are listed according to ascending order of the G/R ratios.

Very different relationships exist between G/R and the two precipitation types. The corresponding means of the G/R values were 0.88 for the high-reflectivity gradient cases (computed from 840 G–R pairs in 25 cases), which indicates a slight radar overestimate, and 2.23 for the low-reflectivity gradient cases (computed from 799 G–R pairs in 18 cases), which indicates a significant radar underestimate. The radar estimated less than half of the gauge-measured accumulations in the low-reflectivity gradient cases.

Brandes et al. (1999) obtained results fairly similar to the high-reflectivity gradient cases discussed above. They compared gauge accumulations with WSR-88D estimates for three precipitation events near Denver, Colorado (June–July 1996), and for nine events near Wichita, Kansas (May–June 1997). The precipitation types in their study were convective storms, most of which were attended by stratiform rain areas. Their analyses procedures were slightly different from those used in the current study. They restricted their comparisons to only gauges located 20–90 km from the radars, only considered reflectivities from the lowest elevation scan (0.5°), and used the average accumulation from several radar bins rather than considering only the bin collocated with the gauge. Their mean G/R values were (1.07) (132 G–R pairs) and 1.05 (377 G–R pairs) for the Denver and Wichita area studies, respectively. These numbers are much closer to the 0.88 for the high-reflectivity gradient cases than the 2.23 for the low-reflectivity gradient cases. This should not be surprising since their storms were convective and would be expected to display high-reflectivity gradient characteristics.

As shown in Table 1, the Oklahoma City (OKC) and Boston (BOS) cases were evenly split between high-reflectivity gradient and low-reflectivity gradient cases; Oklahoma City had five in each category, and Boston had four. In Table 3 the G/R ratios (in ranked order) and means of these values for each of these two sites for each precipitation-type category (as listed in Table 2) are shown.

These values are in good agreement with the trends indicated for all the cases lumped together. Table 3 provides evidence that the differences observed between high-reflectivity gradient and low-reflectivity gradient cases are probably not primarily due to differences of radar hardware or calibration characteristics between WSR-88Ds. Brandes et al. (1999) concluded that for well-maintained radars, the storm-to-storm bias varia-

←

lines at 30° intervals, and state boundaries. The color table on the right depicts the intervals of estimated accumulated precipitation in inches. The maximum accumulation is 4.7 in. (11.94 cm). (b) 1503 UTC. The elevation angle is 0.5°, resolution is 1° × 0.54 n mi (1 km). Maps displayed are state and county boundaries and towns. The color table on the right depicts the intervals of reflectivity in units of dB*Z*. The maximum reflectivity is 54 dB*Z*.

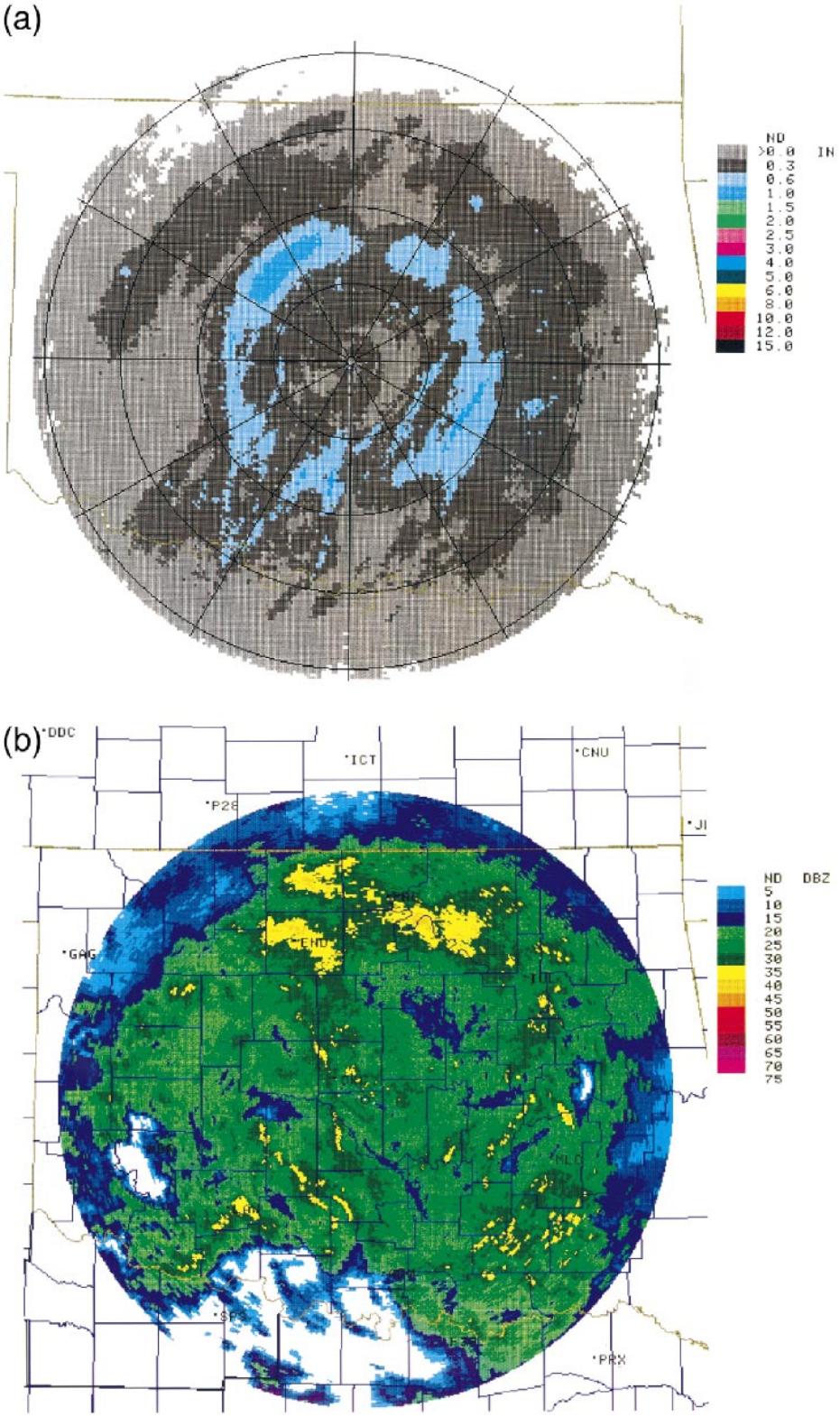

FIG. 2. (a) Oklahoma City, OK, WSR-88D storm total precipitation and (b) base reflectivity products on 29 Apr 1994 for range coverage of 124 n mi (230 km). (a) 1307–2300 UTC. Resolution is 1.1 n mi × 1.1 n mi (2 km × 2 km). Maps displayed are range rings at 30 n mi (55.65 km) intervals, radial sector lines at 30° intervals, and state boundaries. The color table on the right depicts the intervals of estimated accumulated precipitation in inches. The maximum accumulation is 1.3 in. (3.3 cm). (b) 1958 UTC. The

tions due to radar hardware calibration should be small and suggested that differences have a meteorological origin.

The G/R ratio is strongly related to the season (month of occurrence). If the events are subdivided into two groups, 1) June–August and 2) October–January, the corresponding means of the G/R values from Table 2 are 0.79 and 1.82, respectively. In this dataset, the warm season is characterized by high-reflectivity gradient rainfall, and the cool season generally by low-reflectivity gradient rainfall. There were 18 cases classified as high-reflectivity gradient and 0 cases as low-reflectivity gradient during June–August. There were 3 cases classified as high-reflectivity gradient and 11 cases as low-reflectivity gradient during October–January.

a. Variations with distance from radar

The G/R values were computed using Eq. (1) for all cases combined within each precipitation-type classification subdivided into four range categories. The range categories selected were 0–49.9, 50–99.9, 100–149.9, and 150–230 km. These range intervals were subjectively selected to determine general trends of range effects.

The results are shown in Table 4. The G/R ratios greater than 1.00 indicate overall radar underestimation, and ratios less than 1.00 indicate overall radar overestimation.

For high-reflectivity gradient cases, Table 4 exhibits radar underestimation at the nearest ranges and radar overestimation at middle ranges, which decreases with range to a near-zero bias at the farthest range interval.

A much stronger bias as a function of range is evident in the low-reflectivity gradient cases. The radar underestimated rainfall in all four range categories but much more substantially in the nearest and farthest two range intervals where the underestimates exceeded a factor of 2. Radar underestimates were less than a factor of 2 in the second range category. This improvement was probably due to enhanced radar reflectivities from brightband effects.

Table 4 also lists the number of cases from each precipitation type that was represented in each range interval along with the total number of gauge–radar pairs that was considered in the G/R computations. None of the four range intervals had valid gauge–radar pairs from all 25 high-reflectivity gradient or 18 low-reflectivity gradient precipitation events. The number of cases represented ranged from 13 to 23 (high-reflectivity gradient) and 14 to 15 (low-reflectivity gradient). The range interval 0–49.9 km had the fewest gauge–radar pairs in both precipitation-type categories: 101 (12% of the total) for high-reflectivity gradient and 143 (18% of the total) for low-reflectivity gradient.

b. Radar versus gauge scatterplots

Figures 3 and 4 depict comparisons between the radar-estimated accumulations and the corresponding rain gauge amounts for all cases in the high-reflectivity gradient and low-reflectivity gradient categories, respectively. If an exact match occurred, the data point would be plotted along the one-to-one line. However, both radar and rain gauge accumulations could be perfect, and the ratio still could be different from 1.0, since the two sample different processes. Thus there is an uncertainty bound associated with each plotted point due to sampling and other estimation effects. Therefore, the scatterplot, and associated linear regression line and corresponding correlation coefficient will have errors related to these uncertainties and should be viewed as displaying general tendencies and trends rather than precise statistical characteristics.

For the high-reflectivity gradient cases (Fig. 3), the linear regression line is fairly closely aligned with the one-to-one line with only slight underestimation shown and a reasonably good correlation coefficient of 0.74. However, the scatter of data points on either side of the one-to-one line still appears fairly substantial.

The low-reflectivity gradient cases (Fig. 4) exhibit significant underestimation by the radar relative to the gauges. Although the correlation coefficient associated with the linear regression line is a fairly low 0.44, the vast majority of data points lie below the one-to-one line, giving strong evidence that the radar underestimated rain amounts quite consistently.

4. Summary and discussion

Rain gauge measurements were compared with radar-estimated storm total precipitation for 43 rain events that occurred at 10 locations. Gauge-to-radar ratios (G/R) were computed for individual cases and groups of cases.

The G/R ratio is strongly related to precipitation type, with the mean G/R slightly less than 1.00 for high-reflectivity gradient cases and greater than 2.00 (factor of 2 radar underestimation) for low-reflectivity gradient cases. Both precipitation types indicated radar underestimation at the nearest ranges. However, the high-reflectivity gradient cases indicated radar overestimation at farther ranges, while the low-reflectivity gradient cases indicated significant radar underestimation at all ranges.

A possible cause for the underestimation is the typical

←

elevation angle is 0.5°, resolution is 1° × 0.54 n mi (1 km). Maps displayed are state and county boundaries and towns. The color table on the right depicts the intervals of reflectivity in units of dB*Z*. The maximum reflectivity is 44 dB*Z*.

TABLE 2. Summary of radar-estimated vs gauge-measured rainfall accumulations for 10 WSR-88D sites (defined in Table 1). The *G*/*R* ratios were computed by using Eq. (1). Legend for precipitation type: H = high-reflectivity gradient; L = low-reflectivity gradient. "Invalid" means that the case had fewer than nine valid gauge–radar pairs as defined in text. Number of gauges indicates the number of gauges with valid precipitation vs the total number of gauges available in the network.

G/*R* Collocated bin	Site	Precipitation type	Gauge amounts (in.)						Duration	
			Number of gauges	Max	Min	Avg	Med	Std dev	Hours	Dates
0.36	CLE	H	13/27	1.07	0.04	0.33	0.24	0.35	40.5	14–16 Jul 95
0.47	OKC	H	21/85	1.48	0.03	0.27	0.09	0.44	21	23–24 Oct 91
0.51	CLE	H	15/24	0.51	0.04	0.15	0.12	0.14	43.5	16–18 Aug 95
0.52	DEN	H	52/134	0.90	0.03	0.17	0.10	0.17	4	21–22 Jun 94
0.60	DEN	H	90/135	1.95	0.04	0.46	0.32	0.42	2	11 Aug 94
0.68	LBB	H	59/85	1.64	0.03	0.40	0.25	0.41	6	31 Aug 94
0.71	CLE	H	10/31	0.87	0.08	0.40	0.32	0.26	24.5	23–24 May 95
0.71	BOS	H	21/54	0.28	0.03	0.10	0.06	0.07	12	31 Aug–1 Sep 95
0.76	CLE	H	18/24	1.42	0.04	0.32	0.20	0.36	11.5	10–11 Jun 95
0.76	CLE	H	19/24	2.15	0.04	0.68	0.52	0.54	31	24–26 Jul 95
0.78	BOS	H	41/54	2.53	0.04	0.45	0.30	0.51	11	2–3 Aug 95
0.80	NOR	H	68/82	1.85	0.03	0.83	0.76	0.51	21	30–31 Aug 94
0.83	OKC	H	47/47	1.72	0.06	0.82	0.80	0.41	2	9 Jun 93
0.87	BOS	H	51/54	1.75	0.08	0.43	0.24	0.43	36	3–4 Jun 95
0.88	OKC	H	22/85	1.55	0.04	0.35	0.15	0.39	17	25 Jul 91
0.95	CLE	H	17/29	2.29	0.04	0.72	0.56	0.72	11.5	27–28 Jun 95
1.00	CHI	L	33/34	0.61	0.05	0.29	0.29	0.15	24	20–21 Nov 94
1.01	BOS	H	51/54	3.18	0.11	0.54	0.40	0.55	16.5	28–29 Jul 95
1.03	PHX	H	68/158	2.05	0.04	0.30	0.16	0.40	11	18–19 Jul 94
1.04	BOS	L	34/54	0.67	0.11	0.32	0.31	0.12	13	25–26 Sep 95
1.11	HGX	H	56/59	6.13	0.04	1.93	1.68	1.33	23	5–6 May 93
1.17	CHI	L	23/39	0.41	0.09	0.30	0.33	0.10	38	15–16 Dec 94
1.23	OKC	H	42/87	1.13	0.03	0.26	0.14	0.27	18	15 Sep 94
1.24	OKC	H	66/87	3.54	0.04	0.66	0.36	0.75	7.5	4 Nov 94
1.35	CHI	L	35/39	1.29	0.47	0.89	0.88	0.16	38	27–28 Nov 94
1.36	CLE	H	15/25	1.15	0.08	0.50	0.40	0.37	24	26–27 Jul 95
1.36	ATL	L	90/149	1.44	0.04	0.42	0.33	0.30	49	21–23 Dec 94
1.64	CLE	H	18/27	1.32	0.08	0.58	0.26	0.50	25	20–21 Apr 95
1.66	OKC	L	53/87	1.96	0.08	0.72	0.74	0.44	7	2–3 May 94
2.06	BOS	L	14/54	0.74	0.05	0.40	0.33	0.20	17	30 Apr–1 May 95
2.09	OKC	L	78/87	2.03	0.04	0.60	0.50	0.44	19	8–9 Nov 94
2.11	ATL	L	41/87	1.60	0.03	0.44	0.41	0.31	32	30–31 Oct 94
2.18	OKC	L	57/82	1.64	0.04	0.51	0.43	0.36	10	30 Oct–1 Nov 91
2.34	CLE	L	27/27	2.76	0.68	1.61	1.60	0.69	31.5	5–6 Oct 95
2.51	OKC	L	36/70	0.84	0.03	0.24	0.22	0.15	17	30–31 Oct 91
2.72	OKC	L	80/87	2.01	0.23	1.06	1.06	0.33	10	29 Apr 94
2.90	ATL	L	120/124	3.50	0.03	1.09	1.00	0.73	64	12–15 Jan 95
2.98	BOS	L	54/54	3.35	0.84	1.84	1.69	0.57	48.75	20–22 Oct 95
3.92	BOS	L	50/54	1.63	0.48	1.11	1.15	0.29	17.5	8–9 Mar 95
Invalid	CLE	H	10/26	2.14	0.12	0.89	0.88	0.59	22	6–8 Aug 95
Invalid	ATL	H	11/76	0.65	0.03	0.28	0.31	0.20	9	30 Oct 94
Invalid	CLE	L	16/31	0.48	0.03	0.21	0.17	0.13	25	20–21 Mar 95
Invalid	CLE	L	10/27	0.48	0.03	0.23	0.22	0.14	32	3–4 Apr 95

TABLE 3. Gauge-to-radar ratios and corresponding mean value for high- and low-reflectivity gradient cases for Oklahoma City and Boston.

Site	*G*/*R* ratios	Mean
HRG cases		
OKC	0.47, 0.83, 0.88, 1.23, 1.24	0.93
BOS	0.71, 0.78, 0.87, 1.01	0.84
LRG cases		
OKC	1.66, 2.09, 2.18, 2.51, 2.72	2.23
BOS	1.04, 2.06, 2.98, 3.92	2.50

reduction of reflectivity with increasing altitude and the radar beam overshooting the rain clouds (lack of detection) at far ranges that is most evident during cool seasons that are dominated by shallow, stratiform rain systems (Fulton et al. 1998). It is likely that many, and perhaps most, of the 18 low-reflectivity gradient cases in this study were primarily stratiform rain systems, although this was not verified via analyses of vertical structures. Joss and Waldvogel (1989) suggested that significant errors in precipitation estimates can occur when the radar beam scans at higher portions of precipitating systems because vertical reflectivity gradients can be substantial.

This underestimation problem can be exacerbated when the WSR-88D precipitation algorithm incorrectly interprets valid radar echoes in the first tilt (0.5° elevation angle) as ground clutter, subsequently chooses the *second* tilt (1.5° elevation angle) to compute precipitation accumulations, and routinely uses the third and fourth tilt (2.5° and 3.5° elevation angles) near the radar. Smith et al. (1996) reported significant underestimation of rainfall within 40-km range of the WSR-88D radar due to bias in reflectivity observations at higher tilt angles.

The use of an inappropriate *Z*–*R* relationship may also be a significant contributor to the radar underestimates that occurred for the low-reflectivity gradient cases. Better WSR-88D estimates of rain accumulation might result if a stratiform-based *Z*–*R* relationship is used for low-reflectivity gradient precipitation events. The NEXRAD program has already authorized the use of another *Z*–*R* relationship for maritime tropical storms (Fulton et al. 1998).

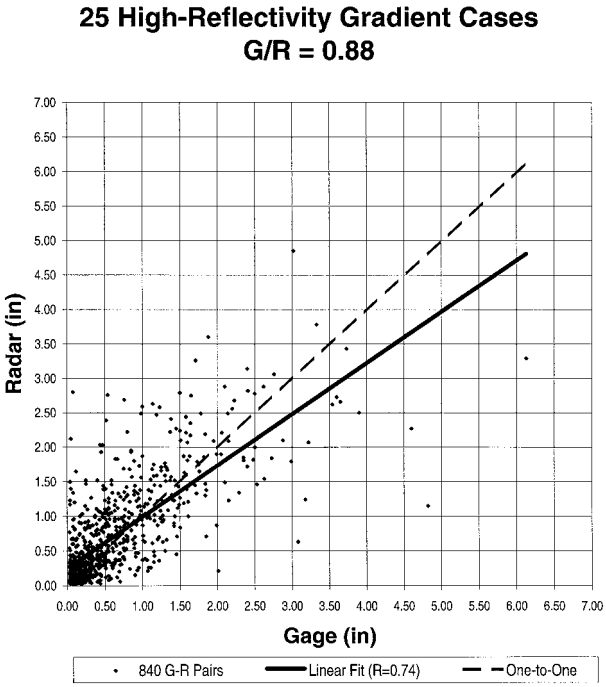

FIG. 3. Scatterplot of radar vs gauge accumulation values for 25 high-reflectivity gradient cases. The one-to-one line (dashed line) is the line of perfect correlation. The *G*–*R* pairs (data points) are all of the gauge–radar pairs in which both the gauge and radar accumulations are greater than 0.03 in. (0.076 cm). Linear fit (solid line) is the linear regression line with the correlation coefficient (*R*) specified in the key.

Variations in *Z*–*R* relationships from storm to storm are expected because of the large number of *Z*–*R* relationships that have been documented, as well as the variations in drop size distributions that occur within a storm (Wilson and Brandes 1979). Brandes et al. (1999) concluded that a primary source of storm-to-storm bias is due to variations in drop size distributions. Future studies to develop improved *Z*–*R* relationships should consider not only gauge measurements and associated observations of radar reflectivity but also measured or computed drop size distributions. Distrometers can be used to measure drop size distributions; however, their sampling volume is quite small compared with the radar sampling volume. Sodars and radar wind profilers can

TABLE 4. *G*/*R* ratios for high-reflectivity gradient (HRG) and low-reflectivity gradient (LRG) precipitation types in four range categories. The *G*/*R* ratios were computed using Eq. (1). Shown are the number of gauge–radar pairs considered in computation of *G*/*R*. Number of cases that contributed gauge–radar pairs out of a total possible of 25 HRG and 18 LRG precipitation events are shown in parentheses.

	Range (km)			
	0–49.9	50–99.9	100–149.9	150–230
G/*R* for HRG	1.18	0.79	0.79	0.97
G/*R* for LRG	2.29	1.57	2.33	2.88
Number of HRG gauge–radar pairs	101	239	256	244
(number of cases)	(13)	(16)	(23)	(22)
Number of LRG gauge–radar pairs	143	197	259	200
(number of cases)	(15)	(15)	(14)	(15)

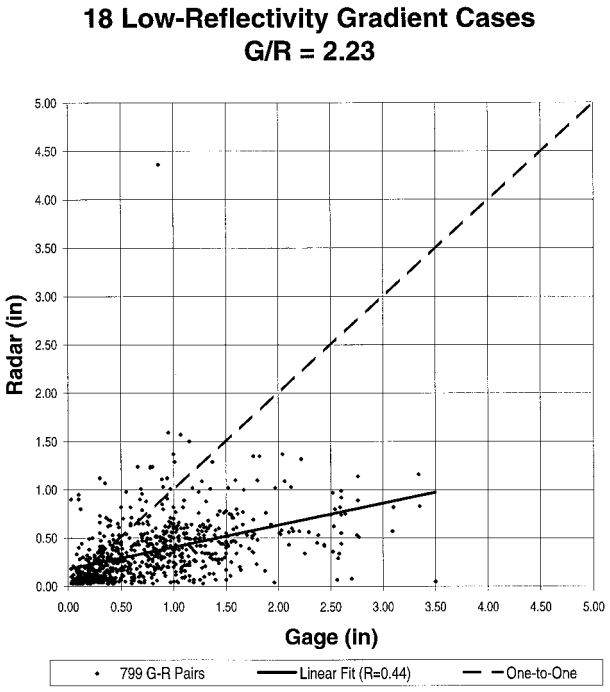

FIG. 4. Same as Fig. 3, except for 18 low-reflectivity gradient cases.

be used to compute drop size distributions, and their sampling volume is more closely aligned with that of the radar (Coulter et al. 1989).

Occurrences of radar overestimates may have been related to high reflectivity returns from melting ice, brightband effects in stratiform systems, and hail from convective systems. Brightband effects probably were responsible for improving the radar underestimates in the second range interval (50–99.9 km) for the low-reflectivity gradient cases. Other possibilities for radar overestimates are anomalous propagation (AP) of the radar beam. Smith et al. (1996) concluded that bright bands and AP can lead to systematic overestimation of rainfall at intermediate ranges.

A potential cause for either radar underestimation or overestimation is improperly calibrated radars. A difference of 4 dBZ corresponds to an approximate doubling or halving of the radar accumulation estimates. For instance, the corresponding precipitation rates from reflectivity measurements of 40 dBZ and 44 dBZ are 12.24 mm h^{-1} (0.48 in. h^{-1}) and 23.63 mm h^{-1} (0.93 in. h^{-1}), respectively, for the WSR-88D default Z–R relationship.

Acknowledgments. Documentation of this work was partially supported by Argonne National Laboratory, which is operated by the University of Chicago for the U.S. Department of Energy under Contract W-31-109-Eng-38.

The authors thank James McCullough for assembling and processing much of the data.

Work on this project was conducted while the authors were employed at or assigned to the NEXRAD Operational Support Facility (OSF) in Norman, Oklahoma. The authors thank James Belville, Tim Crum, Tim O'Bannon, and Andy White at the OSF for their encouragement and support of this project.

The authors thank Howard Johnson of the Oklahoma Climate Survey; the Army Corps of Engineers in Tulsa, Oklahoma; Larry Fayard of the St. John's Water Management District; Lee Czepyha of the Boston National Weather Service Office (NWSFO); Robert LaPlante of the Cleveland NWSFO; Kent Frantz of the Atlanta NWSFO; Ken Labas of the Chicago NWSFO; David Floyd of the Oklahoma City NWSFO; and Nancy Westcott of the Illinois State Water Survey for their assistance in providing radar or gauge data (or both).

The authors thank Arlin Super with the U.S. Bureau of Reclamation for his comprehensive review of the manuscript and very helpful suggestions.

The authors also thank Oak Ridge Institute for Science and Education for providing internships to Jessica M. Thomale and James McCullough through the National Oceanic and Atmospheric Administration's Historically Black Colleges and Universities Student Research Participation Program.

REFERENCES

Brandes, E. A., J. Vivekanandan, and J. W. Wilson, 1999: A comparison of radar reflectivity estimates of rainfall from collocated radars. *J. Atmos. Oceanic. Technol.,* **16,** 1264–1272

Coulter, R. L., T. J. Martin, and T. M. Weckwerth, 1989: Minisodar measurements of rain. *J. Atmos. Oceanic. Technol.,* **6,** 369–377.

Fulton, R. A., J. P. Breidenbach, D. J. Seo, D. A. Miller, and T. O'Bannon, 1998: The WSR-88D rainfall algorithm. *Wea. Forecasting,* **13,** 377–395.

Joss, J., and A. Waldvogel, 1989: Precipitation estimates and vertical reflectivity profile corrections. Preprints, *24th Conf. on Radar Meteorology,* Tallahassee, FL, Amer. Meteor. Soc., 682–688.

Klazura, G. E., and D. A. Imy, 1993: A description of the initial set of analysis products available from the NEXRAD WSR-88D system. *Bull. Amer. Meteor. Soc.,* **74,** 1293–1311.

Manion, J. D., and G. E. Klazura, 1993: A comparison of data from the WSR-88D storm total precipitation product and a network of gages: Preliminary results. Preprints, *26th Int. Conf. on Radar Meteorology,* Norman, OK, Amer. Meteor. Soc., 151–153.

NOAA, 1991: Doppler radar meteorological observations, Part C, WSR-88D products and algorithms. Federal Meteorological Handbook 11, Rep. FCM-H11C-1991, Office of the Federal Coordinator for Meteorological Services and Supporting Research, 210 pp. [Available from National Climatic Data Center, 151 Patton Ave., Rm. 120, Asheville, NC 28801-5001.]

Smith, J. A., D. J. Seo, M. L. Baeck, and M. D. Hudlow, 1996: An intercomparison study of NEXRAD precipitation estimates. *Water Resour. Res.,* **32,** 2035–2045.

Wilson, J. W., and E. A. Brandes, 1979: Radar measurement of rainfall—A summary. *Bull. Amer. Meteor. Soc.,* **60,** 1048–1058.